Title

Numerical Study of Shear Stress Distribution Over Sand Ripples Under Terrestrial and Martian Conditions

Journal

Journal of Geophysical Research Planets, 124(1)

ISSN

2169-9097

Authors

Siminovich, A
Elperin, T
Katra, I
et al.

Publication Date

2019

DOI

10.1029/2018je005701

Peer reviewed

Numerical study of shear stress distribution over sand ripples under terrestrial and Martian conditions

Arik Siminovich [1], Tov Elperin [1], Itzhak Katra [2], Jasper, F. Kok [3], Robert Sullivan[4], Silvestro Simone[5,6] and Hezi Yizhaq[7]

[1] Department of Mechanical Engineering, The Pearlstone Center for Aeronautical Engineering Studies, Ben-Gurion University of the Negev, P. O. B. 653, 8410501, Israel

[2] Department of Geography and Environmental Development, Ben-Gurion University of the Negev, P. O. B. 653, 8410501, Israel

[3] Department of Atmospheric and Oceanic Sciences, University of California, Los Angeles, California 90095, USA

[4]Cornell Center for Astrophysics and Planetary Sciences, Cornell University, Ithaca, NY 14853, USA. (rjs33@cornell.edu)

[5]INAF Osservatorio Astronomico di Capodimonte, Via Moiariello 16, 80131 Napoli, Italy (silvestro@na.astro.it)

[6]SETI Institute, Carl Sagan Center, 189 North Bernardo Avenue, Mountain View, California 94043, USA

[7]Swiss Institutes for Dryland Environmental and Energy Research, BIDR, Ben-Gurion University of the Negev, Midreshet Ben-Gurion, Israel

Keywords: impact ripples, saltation, reptation, ANSYS Fluent, Mars, separation bubble

Abstract

Ripples in a range of sizes occur on Earth and Mars. From terrestrial studies, ripple size is known to depend on grain size-frequency, wind duration, wind strength (including stronger winds that can flatten ripples), as well as fundamental environmental factors that differ between the two planets. Here, we use Computational Fluid Dynamics (CFD) experiments to model boundary layer shear stresses applied to aeolian ripple surfaces, to investigate how these stresses might differ between Earth and Mars. CFD

experiments used ANSYS Fluent, with inlet wind speeds of 10 m/s and 15 m/s for both planetary environments. Ripple profiles for Earth and Mars were developed using saltation and reptation properties modeled by the numerical saltation model COMSALT (Kok and Renno, 2009) to develop ripple profiles using the numerical technique of Yizhaq et al. (2005). Although the CFD experiments using these inputs could not include the effects of a saltation cloud, results are robust enough to indicate clearly that for similar modeled wind speeds on Earth and Mars, boundary layer shear stress applied to ripple surfaces is greater on Earth. This indicates that fluid shear stress is a more important factor for controlling ripple size on Earth than on Mars.

1. Introduction

Impact or normal ripples are common on Earth and Mars and are generated due to the instability of a flat bed to the action of the wind on loose sand (Fig. 1). They develop on fine sand with a unimodal distribution, unlike megaripples which require a bimodal distribution to form (Yizhaq et al., 2012; Lämmel et al., 2018). Their wavelength on Earth is <30 cm and their height is less than 1 cm, whereas on Mars they might be much larger both in wavelength and height (Sullivan et al., 2008; Bridges et al., 2012; Lapotre et al., 2016; Silvestro et al., 2016; Ewing et al., 2017). On Mars, two sizes of aeolian ripples were observed, small (decimeter scale) impact ripples like on Earth (Sullivan et al., 2005; Yizhaq et al., 2014) and large, meter scale ripples with no terrestrial analog (Bridges et al., 2012; Laoptre et al., 2016; Ewing et al., 2017). The large ripples on Mars were detected in orbital images (Malin and Edgett, 2001; Bridges et al., 2007) and first visited *in situ* by the NASA Mars Exploration Rover (MER) Spirit at the El Dorado ripple field in Gusev Crater (*Sullivan et al.*, 2008]). Based on recent data sent by the NASA Mars Science Laboratory (MSL) Curiosity in Gale Crater, Lapotre et al. (2016)

gave an alternative hypothesis for the origin of the large (2.1 meter in wavelength) ripples that superimpose the dune slopes. According to their theory, the large ripples visited by Curiosity are fluid drag ripples (Bagnold, 1941; Wilson, 1972) which form due the large kinematic viscosity on Mars (Lapotre et al., 2016). In this scenario, the large Martian ripples are not just larger version of the terrestrial impact ripples, but rather analogues to current ripples [Allen, 1968] which form in unidirectional water streams on Earth (Lapotre et al., 2016). These large ripples cannot be megaripples because there is no discernable grain size variation between the crest and slopes of the ripple (Lapotre et al., 2016; Ewing et al., 2017), thus they form unique bedform. However, based on numerical simulations for wind velocity near the threshold, Durán et al. (2014) predicted that the ripple wavelength on Mars can be 20 times larger than impact ripples on Earth. Assuming a typical wavelength of terrestrial ripples as 0.15 means that ripples on Mars can grow up to 3 m wavelength without the need of explaining their dimensions with the fluid drag theory.

Ripples form when the wind speed exceeds a certain threshold and sand grains begin to move, mostly through saltation and reptation (Kok et al., 2012). The motion of grains transported by saltation is composed of a series of asymmetric ballistic trajectories which are accelerated by the wind and upon hitting the bed they eject low energy grains. These grains move in small jumps close to the surface through a mode of transport known as reptation (Anderson, 1987; Durán et al., 2014).

The ripple dimensions (height and wavelength) grow in time until reaching an equilibrium where the growing ceases and the ripples only drift downwind with a velocity (celerity) which is linearly dependent on wind speed (Andreotti et al., 2006, Rasmussen et al., 2015). In this state the deposition of grains at the crest is balanced by erosion due the speedup of wind velocity at crest (Bar et al., 2016). The steady state

dimension of ripples depends on the wind velocity and on the grain diameter (Bagnold, 1941; Sharp, 1963; Seppälä and Lindé, 1978; Anderson, 1987; Andreotti et al., 2006; Durán et al., 2014; Schmerler et al., 2016).

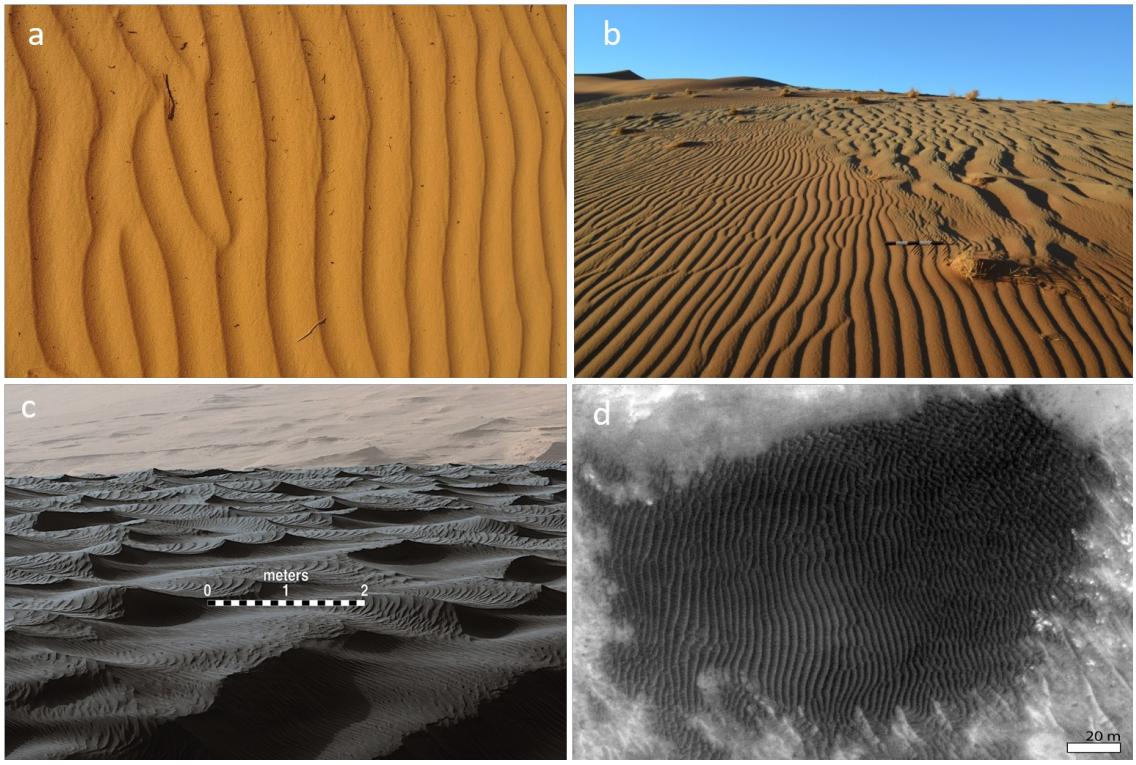

Figure 1. Ripples on Earth and Mars. (a) Normal ripples at Nizzana sand dunes at the western Negev near the border between Israel and Egypt. (b) A sharp transition between almost straight normal ripples (right) and wavy megaripples (left) on the downwind slope of a dune at Sossusvlei, Namibia (the scale bar is 0.5 m long). (c). Two sizes of ripples are evident in this Dec. 13, 2015, view of a top of a Martian sand dune, from NASA's Curiosity Mars rover. (d) Large straight normal ripples in Gusev crater, Mars.

Due to the low density on the surface of Mars the fluid shear velocity u_{*t} needed for direct entertainment of grains into saltation is much higher than on Earth (Fig 2;

Greeley et al., 1980; Iversen and White, 1982; cf. Shao and Lu, 2000; Kok 2010a; Kok 2010b; Kok et al., 2012). However, on Mars there is a big discrepancy between the fluid threshold to the impact threshold u_{*ti}, which is the shear velocity needed to sustain saltation by the impact mechanism (Kok, 2010b: Yizhaq et al., 2014). On Earth the ratio $u_{*ti}/u_{*t} : 0.8$ while on Mars it is $u_{*ti}/u_{*t} : 0.1$ (Kok et al., 2012). It was suggested that this difference can explains the large aeolian activity observed on Mars despite the low predicted wind velocities (Kok, 2010b; Kok et al., 2012; Silvestro et al., 2011; Sullivan and Kok, 2017). GCM models for Mars generally do not predict $u_* > u_{*t}$ and thus no sand transport should occur (Basu et al., 2004; Chojnacki et al., 2011). Sporadic and limited wind measurements made by Mars landers have also found that winds on Mars rarely exceed the fluid threshold (Schofield et al., 1997; Zimbelman, 2000; Holstein-Rathlou et al., 2010). Recently it was suggested that sand transport on Mars could occur close to u_{*ti} without the need of gusts above the fluid threshold to initiate the saltation (Sullivan and Kok, 2017).

The goal of this paper is studying the distribution of shear stress τ and shear velocity u_* (a measure of the wind stress defined as $u_* = \sqrt{\tau / \rho_a}$ where ρ_a is the air/atmosphere density) over simulated ripples produced by a mathematical model under terrestrial and Martian conditions for two moderate wind speeds (10 and 15 m/s).

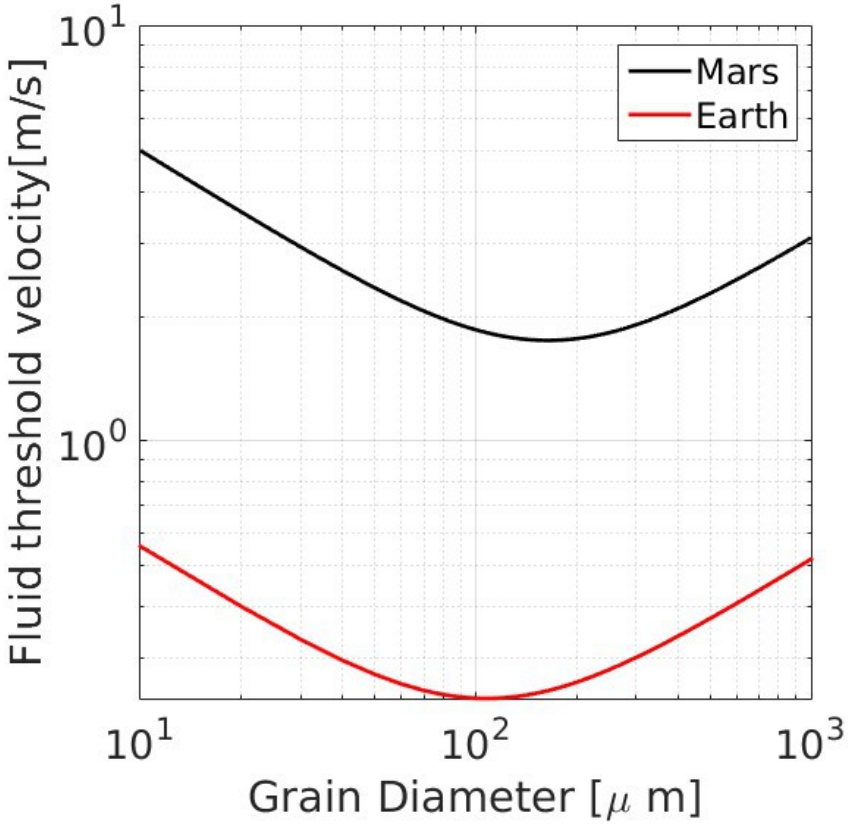

Figure 2. Fluid threshold velocity as a function of grain size for Earth (red) and Mars (blue) conditions. Both curves show a minimum around 100 µm. The calculations are based on Shao and Lu, 2000. Note that the Martian fluid threshold velocity is much higher than that on Earth.

2. Methods

2.1 Ripple model

To produce the ripples profiles for Earth and Mars we used the COMSALT model for saltation (Kok and Renno, 2009) together with a dynamic 2D model for sand ripples (Yizhaq et al., 2004) in the same method used in Yizhaq et al., (2014).

COMSALT includes many of the advances of previous models (e.g. Werner, 1990), and in addition it includes: (1) a physically based parameterization of the splashing of

surface particles that agrees with experimental and numerical studies (Kok and Renno, 2009), (2) a generalization of this splashing process to beds of mixed particle sizes, and (3) a detailed treatment of the influence of turbulence on particle trajectories, which agrees with laboratory measurements. Because of these and other advances, COMSALT is the first physically-based numerical saltation model to reproduce a wide range of experimental data. Result of the indicate that saltation can be maintained on Mars by wind speeds an order of magnitude less than those required to initiate it (Kok, 2010b).

We used COMSALT to give the values of the parameters for saltation and reptation on Earth and Mars that were used by the ripple model, specifically: the average number of reptating grains per impact of one saltating grain, the number density of saltator impacts on a flat surface, and the probability distribution of reptation lengths.

The ripple model is based on the classic approach of Anderson (1987) and includes a correction to the reptation flux that depends on the local bed slope (Yizhaq et al., 2004). According to Anderson's model, the sole role of saltating grains is to bring energy into the system, extracting it from the wind that blows above the surface of the sand. Within this view, ripple formation is due entirely to spatial changes in the reptation flux. We thus built a 2D dimensional model of sand transport based on the Exner equation (Yizhaq et al., 2004):

$$(1-\lambda_p)\rho_p \frac{\partial h}{\partial t} = -\frac{\partial Q}{\partial x}, \qquad (1)$$

where $h(x,t)$ is the local height of the sand surface at point x and time t, λ_p is the porosity of the bed (taken as 0.35), ρ_p is the grain density and $Q(x,t)$ is the sand flux, which includes both saltation and reptation flux. Here, we assume that saltation flux can be

taken as uniform and we do not take it into consideration in the Exner equation (for a different view of this point see Durán et al., 2014). Thus, in Eq. 1 we take into account only the reptation flux, Q_r. The reptation flux at a certain point and time is obtained by the sum of all the grains that pass that point at that time. The grains have a probability distribution of reptation lengths $p(\alpha)$. Following Anderson (1987), we derive an explicit expression for the reptation flux:

$$Q_r = mn\int_0^{\infty} d\alpha\, p(\alpha) \int_{x-\alpha}^{x} N_{im}(x')dx \quad , \qquad (2)$$

where m is the mass of each particle, n is the average numbers of reptating grains ejected by the impact of one saltating grain, and $p(\alpha)$ is the probability distribution of reptating grains. Because saltation flux is uniform and the fixed angle ϕ at which the grains descend back to the ground is assumed to be constant, the number density of impacting grains changes only because of variations in bed slope. Based on geometrical considerations, we obtain,

$$N_{im}(x) = N_{im}^0 \frac{1+h_x \cot\phi}{\sqrt{1+h_x^2}}, \qquad (3)$$

where h_x is the local slope and N_{im}^0 is the number density of impacting grains on a flat surface. We further modify Eq. (3?) to take into account the correction of the reptation flux on an inclined plane (Yizhaq et al, 2004). This correction leads to a reptation flux

that is smaller on the windward slope and larger on the leeward slope of the bedform. The full model can be written as:

$$h_t = -Q_0 \partial_x \left[(1-\mu) Q_r \right], \quad (4)$$

where the parameter μ heuristically includes the correction to reptation flux discussed above, and $Q_0 = mnN_{im}^0 \cot\phi / \rho_b (1-\lambda_p)$. The basic parameters ($N_{im}^0, n, p(\alpha)$) used in the model are given by COMSALT, which simulates Martian and Earth conditions for $u_* = 0.5$ m/s and for 100 μm (see Yizhaq et al, 2014). The computed probability distribution of reptation lengths is given by

$$p(\alpha) = s(1-\exp(-\sqrt{x/a}))(b/x)\exp(-\sqrt{x/c}), \quad (5)$$

where s, a, b, c are numerical constants (see Table 1) and $\int_0^\infty p(\alpha) d\alpha = 1$.

	N_{im}^0	n	$p(\alpha)$
Earth	132125000	0.7288	$a = 7.81 \times 10^{-5}$ $b = 0.17$ $c = 0.0235$ $s = 1.564$
Mars	1750200	1.1748	$a = 0.00039$ $b = 0.215$ $c = 0.027$ $s = 1.241$

Table 1: The parameters used in the ripple simulations, which were calculated by COMSALT model.

The ripple model equation (Eq. 4) was solved numerically by using an explicit second-order finite difference scheme with periodic boundary conditions starting from random initial conditions. The integral terms were computed by using the composite trapezoid rule, and the time integration was carried out by using the second-order Adams-Bashforth rule (Fausett, 1999). The grid was comprised of 2048 points for a spatial dimension of 2 m (i.e., spatial resolution of approximately 1 mm) and a time step of 0.005 s. The wind velocity and wind direction are assumed to be constant during the simulation and are expressed in the model by the calculated COMSALT parameters values. Although ripples on Earth can be formed within minutes (Anderson, 1990; Andreotti et al., 2006), the lower Martian air density results in a much lower saltator

impact rate (~two order of magnitudes) on Mars (~10^6 m^{-2} s^{-1} for $u_* = 0.5$ m/s) than on

Earth (~10^8 for $u_* = 0.5$ m/s), making the Martian ripple formation much slower.

CFD method 2.2

In the numerical study of the shear stress over the ripples we used ANSYS Fluent (see ANSYS Manual). The details of the implementation of the numerical code are elaborated below.

2.2.1 Geometry and meshing

We considered a two-dimensional rectangular control volume with a height of 1 m and a width (i.e. the length in the direction parallel to the shearing flow) of 12 m. The control volume is divided into two sections in the flow direction: a section with ripples along 7 m and a smooth plate having a length of 5 m. The geometry was chosen such that the control volume is short enough to be numerically efficient with reasonably fine mesh

while long enough to ensure that the mean flow and the small-scale flow features in the vicinity of the ripples do not change appreciably along the direction of the flow. The upper boundary of the control volume is a non-moving smooth wall, while the bottom is a non-moving wavy wall shaped by a periodic pattern of ripples. The basic form of ripples is asymmetric and shown in Fig. 3. Their shapes were taken from the numerical simulations of the ripple model described above. The inlet boundary condition is posed at the left boundary of the control volume while the outlet boundary condition is posed at the right boundary of the control volume. In constructing the mesh, we used an adaptive mesh which is refined in the vicinity of the wavy wall in order to capture fine features of the flow. The mesh consists of quadrilateral and triangular plane elements.

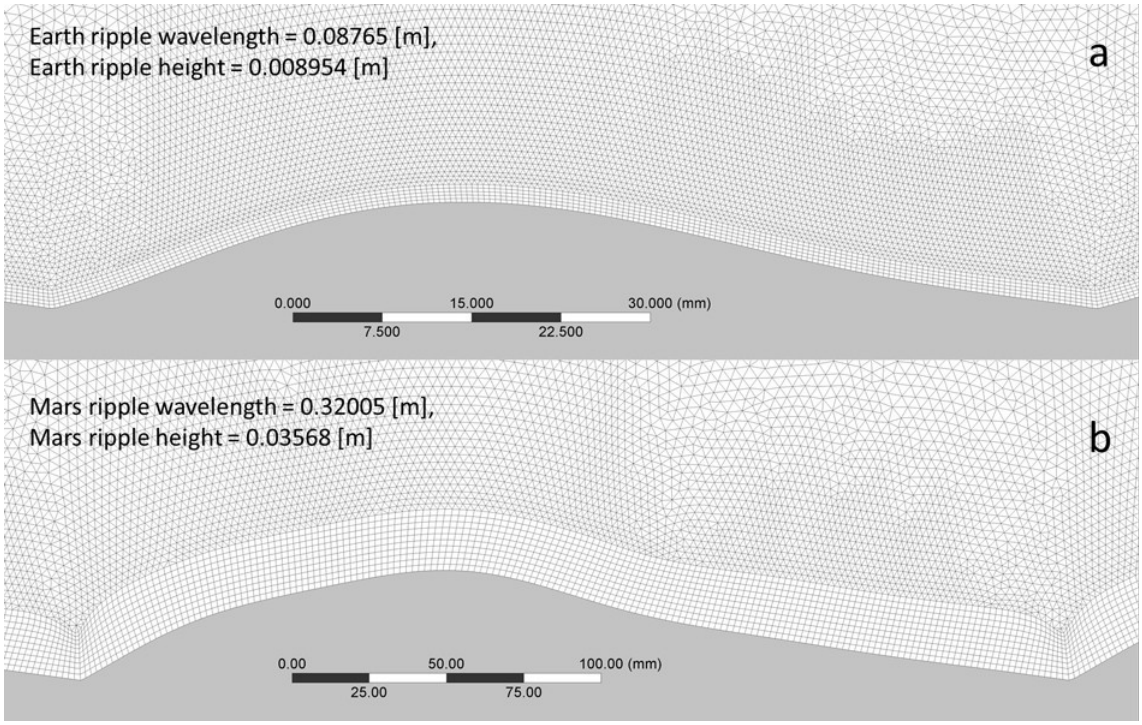

Figure 3. The two profiles used in the ANSYS Fluent simulation for Earth (a) and for Mars (b). The profiles were produced by numerical simulations of the ripple model (Eq. 1). Note that the Martian ripple is larger (in both height and wavelength) than the terrestrial ripple.

2.2.2 Setup and solution

In the numerical solution we used a steady-state density-based two-dimensional solver. The parameters for Earth and Mars atmospheres are presented in Table 2 (see Kok et al., 2012). At the upper and bottom boundaries of the computational domain we posed no-slip solid wall boundary conditions for velocity, and constant temperature pertinent for Earth and Mars atmospheres on the walls. At the inlet we defined a uniform normal-to-plane flow with turbulent intensity of 5% and turbulent viscosity ratio of 10. In the simulations we employed the SST (shear stress transport) k-omega turbulence model (see e.g. Menter (1994)) since the main goal of this study is to determine the shear stress distribution at the wall. As in all turbulence models, the SST model has a number of parameters which must be specified. In the calculations we used the default values of these parameters in ANSYS Fluent. In order to ensure full convergence for the density-based solver, we used the solution steering option that is a solver convergence tool in ANSYS Fluent for density-based steady-state solutions. The blending parameter in the steering option determines the ratio of the second-order blending accuracy to the first-order accuracy of the discretization schemes. In the simulations we used a blending parameter of 75%. The rest of the parameters used with the steering option were the default values. In the calculations we used the equation of ideal gas as equation of state for atmospheres of Earth and Mars. The density-based solver solves the energy conservation equation together with momentum and mass conservation equations. It should be emphasized that we considered a single phase flow over a rough surface with no regard to the influence of the saltating sand grains on the flow.

	$T[$	$g\left[\frac{n}{s}\right.$	$P[Pa$	$\rho\left[\frac{kg}{m^3}\right]$	$C_p\left[\frac{J}{Kg}\right.$	$k\left[\frac{W}{m\cdot}\right.$	$\nu\left[\frac{m^2}{s}\right]$	$\mu\left[\frac{kg}{m\cdot s}\right]$	$m_w\left[\frac{kg}{Km}\right.$

Ear	29	9.81	1013	1.205	1005	0.025	$15.11 \cdot 1$	$1.8208 \cdot 1$	28.966
Ma	21	3.71	600	0.0146	743.246	0.025	$6 \cdot 10^{-4}$	$1.2 \cdot 10^{-5}$	43.34

Table 2. The parameters for Earth and Mars atmospheres used in the ANSYS Fluent simulations.

2.2.3 Code validation

Numerical results were compared with the known analytical solutions for the laminar and turbulent flow over a flat plate under Earth ambient pressure?. Mesh verification was made in order to ensure high mesh quality. We verified that the mesh is dense enough to resolve the fine structure of the flow in the vicinity of the ripples in the region with the wall coordinate $y^+ = yu_* / \nu < 10$ (for details see Landau and Lifshitz, p. 175, Fig. 31) where ν is the fluid's kinematic viscosity for air (see Table 2)).

3. Results

Shear stress and shear velocity distribution over the ripples for Earth and Mars for inlet wind velocities of 10 and 15 m/s are shown in Figs. 4 and 5, respectively.

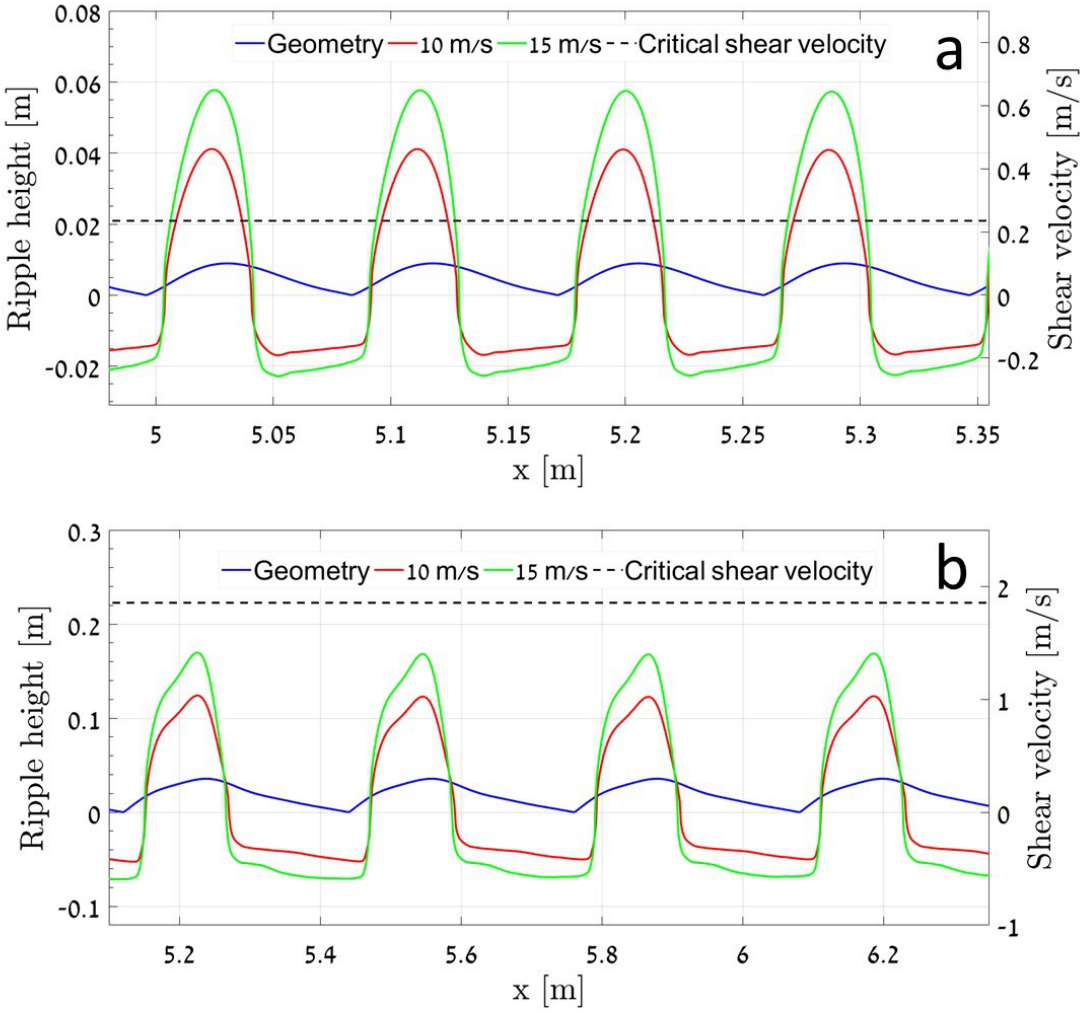

Figure 4. Shear velocity over the ripples (in blue) for two wind velocities 10 m/s (red) and 15 m/s (green) for Earth (a) and Mars (b). The dashed line shows the calculated fluid shear velocity threshold velocity based on Shao and Lu, 2000 for 100 μm particles. For Earth conditions the shear velocity is above the fluid threshold velocity at the crest and at part of the windward slope, whereas under Mars conditions $u_* < u_{*_t}$ for the entire ripple profile.

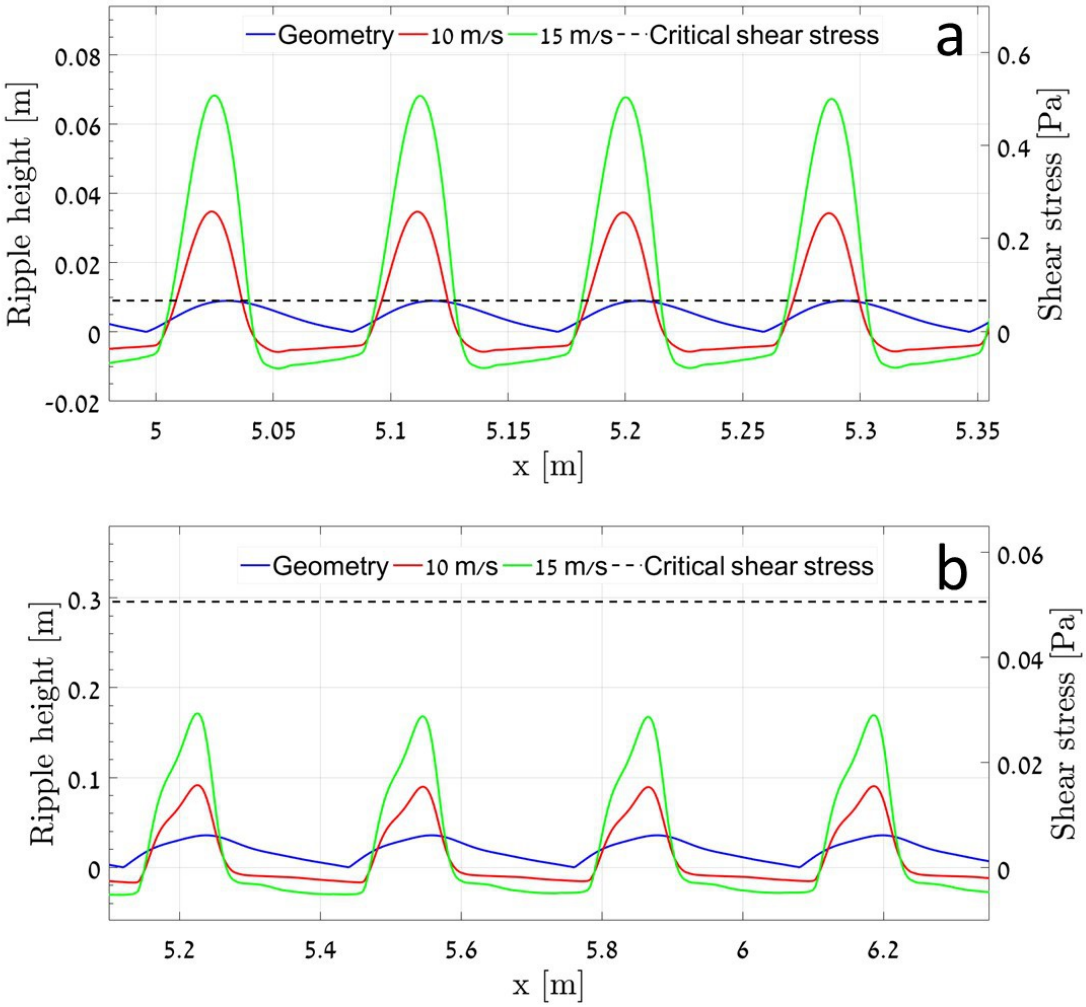

Figure 5. Shear stress over the ripples (in blue) for two wind velocities 10 m/s (red) and 15 m/s (green) for Earth (a) and Mars (b). The dashed line shows the calculated shear stress threshold based on Shao and Lu, 2000 for 100 μm particles. For Earth conditions the shear stress is above the fluid threshold velocity at the crest and at part of the stoss slope, whereas for under Mars conditions the shear stress is below the threshold.

The interesting fine features of the flow are the vortices between the neighboring ripples (Figs. 6 and 7). Clearly, the emergence of the vortices depends on the geometry of the ripples and the incoming flow velocity and fluid parameters. The flows with the vortices are similar to those observed in flows over a cavity or like the separation bubble over

barchans dune (Herrmann et al., 2005). Evidences for the existence of such vortices above ripples were found in wind tunnel experiments by Tong and Huang (2012).

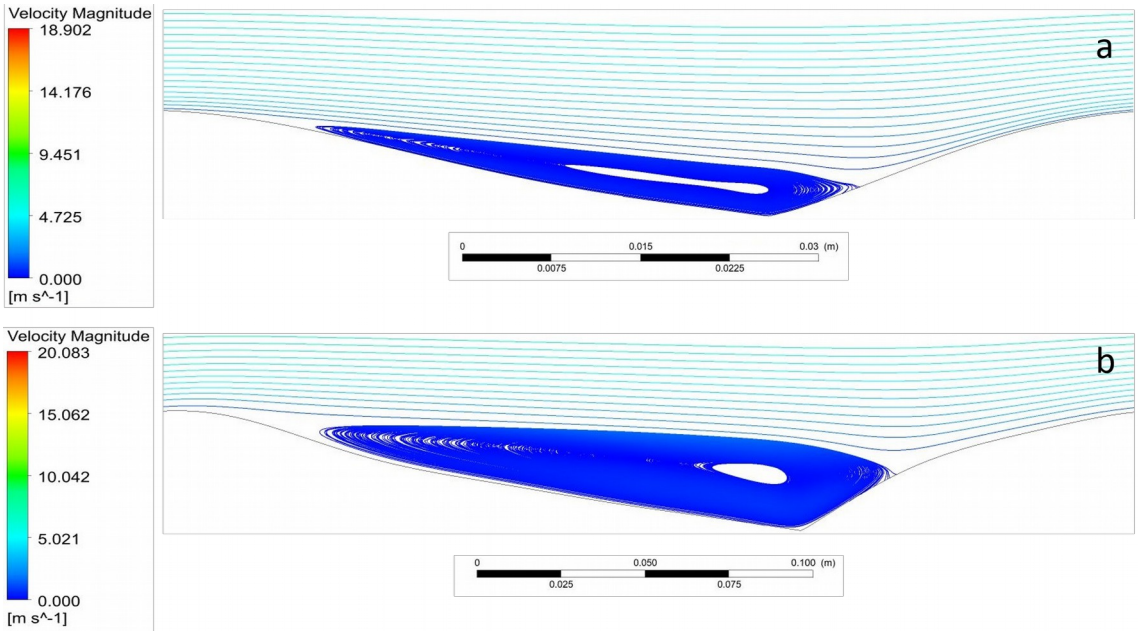

Figure 6. Close up of the vortices that formed between successive ripples for Earth (a) and mars (b) for 15 m/s wind speed.

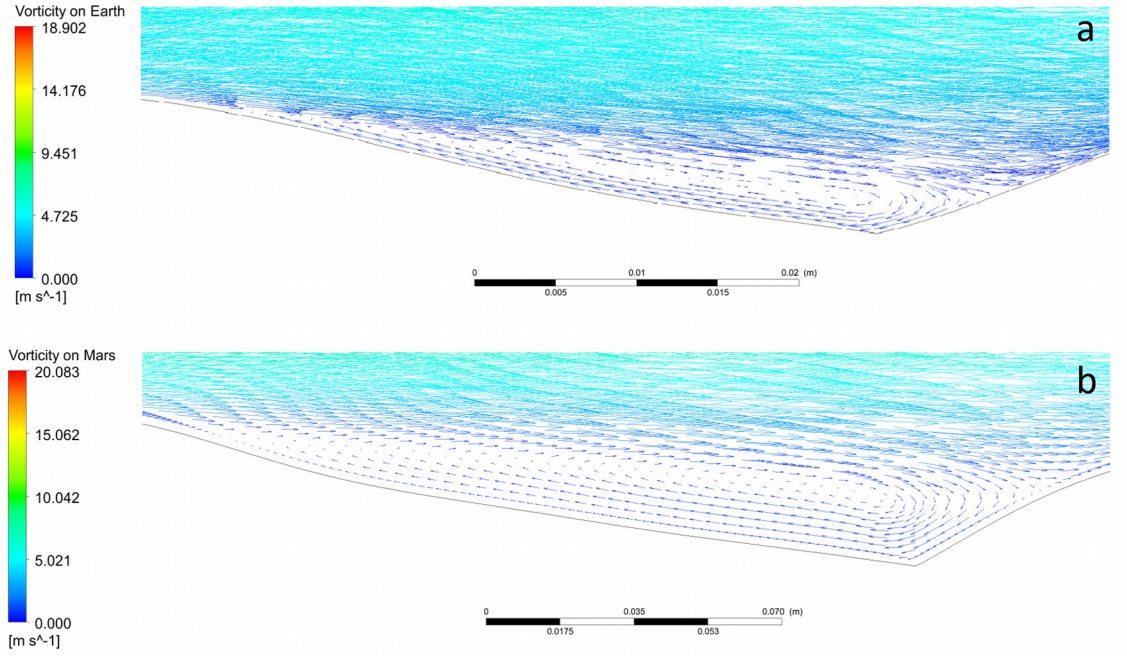

Figure 7. Streamlines of the flow inside the trough between two successive ripples for Earth (a) and mars (b) for 15 m/s wind speed from left to right.

4. Discussion

In the current study we show by ANSYS Fluent CFD simulations over sand ripples that the shear stress above the ripple crest on Mars is below the shear stress needed to drive the grains from the crest into saltation. Contrary to Mars, the CFD simulations over smaller terrestrial ripples show that the shear velocity at the crest is above the fluid threshold. It is important to note that our analysis does not account for the effect of the saltation cloud, which will decrease the shear stress at the surface (REFS). Thus, our results overestimate the shear stress during saltation. This effect is much more significant for Earth than for Mars where the sand flux is generally an order of magnitude smaller (Chojnacki et al., 2016). In addition, the saltation flux on Mars will further reduce the simulated shear velocity over the ripples, thus our results suggest that, for the simulated wind speed, no direct entertainment would occur from the ripple crests.

The simulated shear stress distribution over the terrestrial simulated sand ripples is more important at the initial phase of saltation, before the development of steady state saltation, when the effect of the saltation layer on surface stress is small. At this transient stage, sand grains from the crests will be dislodged as the shear stress at the surface is larger than the fluid thresholds, thus decreasing ripple height.

Future works should include the effect of the saltation layer on the flow and CFD simulations of shear stress over large ripples like the ones found by Curiosity at Gale

Crater (Lapotre et al., 2016) and for more common sand grain sizes, e.g. 200 and 300 μm.

5. Conclusions

The existence of large impact ripples on Mars lacking appropriate terrestrial analogues is not fully understood and it is still in debate (Vaz et al., 2017; Lapotre et al., 2018; Sullivan et al., 2018).

ANSYS Fluent CFD simulations over simulated sand ripples show that the shear velocity above ripple crest on Mars is below the shear stress needed to drive the grains from the crest into saltation for inlet velocities of 10 and 15 m/s. Our results are very important for understanding aeolian processes involved in ripples formation under Martian atmospheric conditions. Further studies are needed to verify this conclusion for more realistic larger Martian ripples and for higher shear velocities.

Acknowledgments

This work was supported by the German-Israeli Foundation for Scientific Research and Development (GIF Research grant 1143-60.8/2011), and by NASA's Outer Planets Research Program (grant 131186).

References

Allen, J. R. L. (1968), Current Ripples: Their Relation to Patterns of Water and Sediment Motion, North-Holland Pub. Co.

Anderson, R S., 1987. A theoretical model for aeolian impact ripples. Sedimentology, 34, 943-5.

Anderson, R. S., 1990. Eolian ripples as examples of self-organization in geomorphological systems. Earth-Science Reviews, 29, 77-96.

Andreotti B., Claudin, P. and Pouliquen, O., 2006. Aeolian sand ripples: experimental study of fully developed states. Physical Review Letters. 96, doi:028001.

Bagnold, R.A., 1941. The Physics of Blown Sand and Desert Dunes. Methuen, London.

Basu, S., Richardson, M. I. and Wilson, R.J., 2004. Simulation of the Martian dust cycle with GFDL Mars GCM. Journal of Geophysical Research, 109, E11006, doi:10.1029/2004JE002243.

Bar, N, Elperin, T., Katra, I., Yizhaq, H., 2016. Numerical study of shear stress distribution at sand ripple surface in wind tunnel flow. Aeolian Research, 21, 125-130.

Bridges, N.T, Ayoub, F., Leprince, S., Lucas, A. and Mattson, S., 2012. Earth-like sand fluxes on Mars. Nature, Doi:10.1038/nature11022.

Chojnacki, M., Burrm D. M., Moersch, J. F and Michaeles, T. I., 2011. Orbital observations of contemporary dune activity in Endeavor Crater, Meridiani Planum, Mars. Journal of Geophysical Research, 116, E00F19, doi:10.1029/2010JE003675.

Chojnacki, M., A. Urso, L. K. Fenton, and Michaeles, T. I., 2016. Aeolian dune sediment flux heterogeneity in Meridiani Planum, Mars, Aeolian Res., doi:10.1016/j.aeolia.2016.07.004.

Durán, O., Claudin, P. and Andreotti, B., 2014. Direct numerical simulations of aeolian sand ripples. PNAS 111 (44) 15665-15668.

Ewing, R. C., et al. 2017. Sedimentary processes of the Bagnold Dunes: Implications for the eolian rock record of Mars, J. Geophys. Res. Planets, 122, doi:10.1002/2017JE005324.

Greeley, R., Leach, R., White, B., Iversen, J., and Pollack, J. B., 1980, Threshold wind speeds for sand on Mars: Wind tunnel simulations, Geophysical Research Letters, 7(2), 121-124.

Greeley, R., and Iversen, J. D., 1985. Wind as a Geological Process on Earth, Mars, Venus, and Titan, Cambridge Univ. Press, New York.

Haberle, R.M., Houben, H.C., Hertenstein, R. and Herdtle, T., 1993. A boundary-layer model for Mars: comparison with Viking lander and entry data. Journal of Atmospheric Sciences, 50, 1544-1559.

Herrmann, H.J., Andrade, J.S., Schatz, V., Sauermann, G., Parteli, E.J.R., 2005. Calculation of the separation streamlines of barchans and transverse dunes. Phys. A 357, 44–49.

Holstein-Rathlou, C., et al, 2010. Winds at the Phoenix landing site J. Geophys. Res., 115, E00E18.

Iversen, J. D., and White, B. R., 1982, Saltation thresholds on Earth, Mars, and Venus, Sedimentology, 29, 111-119.

Fausett, L. V., 1999. Applied Numerical Analysis Using Matlab. Prentice Hall, Upper Saddle River, NJ 07458.

Kok, J. F. and Renno, N.O., 2009. A comprehensive numerical model of steady state saltation (COMSALT). Journal of Geophysical Research, 114, D17204. doi:10.1029/2009 JDO11702.

Kok, J. F. 2010a. An improved parameterization of wind-blown sand flux on Mars that includes the effect of hysteresis. Geophysical Review Letters, 37, doi:L12202.

Kok, J. F., 2010b. Differences in the wind speeds required for initiation versus continuation of sand transport on Mars: Implications for dunes and sand storms. Physical Review Letters, 104, doi:074502.

Kok, J. F., Parteli, E. J. R., Michaels, T. and D. Bou Karam, 2012. The physics of wind-blown sand and dust. Reports on Progress in Physics, 75, 106901.

Lämmel, M., Meiwald, A., Yizhaq, H., Tsoar, H., Katra, I. and Kroy, K. 2018. Aeolian sand sorting and megaripple formation, *Nature Physics*. DOI: 10.1038/s41567-018-0106-z.Landau, L. D., and Lifshitz, E. M., 1999. Fluid Mechanics. Butterworth-Heinemann, Oxford.

Lapotre, M. G. A. et al., 2016. Large wind ripples on Mars: A record of atmospheric evolution. Science, 353, 6294, 55–58, doi:10.1126/science.aaf3206.

Lapotre, M. G. A., Ewing, R. C., Weitz, C. M., Lewis, K. W., Lamb, M. P., Ehlmann, B. L. and Bridges, N. T., 2018. Morphologic diversity of Martian ripples: implications for low-intensity transport as a mechanism for large-ripple formation, in X International Conference on Aeolian Research.

Menter, F. R., 1994. Two-equation eddy-viscosity turbulence models for engineering .applications. AIAA Journal, **32**, 1598-1605

Rasmussen, K. R., Valance, A. and Merrison, J., 2015. Laboratory studies of aeolian sediment transport processes on planetary surfaces. *Geomorphology*, 244, 74-94.

Schofield, J.T., Barnes, J.R., Crisp, D., Haberle, R.M., Larsen, S., et al., 1997. The Mars Pathfinder atmospheric structure investigation meteorology (ASI/MET) experiment. Science 278, 1752–1758.

Seppälä, M., and Lindé, K. (1978). "Wind tunnel studies of ripple formation."Geografiska Annaler. Series A. Physical Geography: 29-42.

Shao, Y., Lu, H., 2000. A simple expression for wind erosion threshold friction velocity. Geophysical Research Journal 105, 22437-22443.

Sharp, R. P., 1963. Wind ripples. Journal of Geology, 71, 617-636.

Schmerler, E., Katra, I., Kok, J.F., Tsoar, H., Yizhaq, H. (2016) Experimental and numerical study of Sharp's shadow zone hypothesis on sand ripple wavelength. Aeolian Research 22, 37-46.

Silvestro, S., Fenton, L. K., Vaz, D. A., Bridges, N. T., and Ori, G. G., 2010 Ripple migration and dune activity on Mars: Evidence for dynamic wind processes, Geophysical Review Letters, 37, L20203, doi:10.1029/2010GL044743.

Silvestro, S. D. A. Vaz, L. K. Fenton, P. E. Geissler, 2011. Active aeolian processes on Mars: A regional study in Arabia and Meridiani Terrae. Geophysical Research Letters., 38, L20201, doi:10.1029/2011GL048955, 2011.

Silvestro, S., Vaz, D. A., Yizhaq, H., Esposito, F. 2016. Dune-like dynamic of Martian Aeolian Large Ripples. Geophysical Research Letters., 43, 8384–8389, doi:10.1002/2016GL070014.

Sullivan, R., Banfield, D., Bell III, J.F., al., 2005. Aeolian processes at the Mars Exploration Rover Meridiani Planum landing site, Nature, 436, doi: 10.1038/nature03641.

Sullivan, R., Arvidson, R., Bell III, J.F., et al., 2008. Wind-driven particle mobility on Mars: Insights from Mars Exploration Rover observations at “El Dorado” and

surroundings at Gusev crater, J. Geophys. Res., 113, E06S07.Sullivan, R., and Kok, J. F. 2017.Aeolian saltation on Mars at low wind speeds, J. Geophys. Res. Planets, 122, 2111–2143, doi:10.1002/2017JE005275.

Sullivan, R., J., Kok, J. F., Yizhaq, H., Siminovich, A., Elperin, T. and Katra, I. (2018).

Low dynamic wind pressures on Mars allow a broad continuum of aeolian ripple sizes, in X International Conference on Aeolian Research.

Tong, D., Huang, N., 2012. Numerical simulation of saltating particles in atmospheric boundary layer over flat bed and sand ripples. J. Geophys. Res.: Atmos., 1984–2012.

Vaz, D. A., S. Silvestro, P. T. K. Sarmento, and M. Cardinale (2017), Migrating meter-scale bedforms on Martian dark dunes: Are terrestrial aeolian ripples good analogues?, Aeolian Res., 26, 101–116, doi:10.1016/j.aeolia.2016.08.003.

Werner, B. T., 1990. A steady-state model of wind-blown sand transport. Journal of Geology, 98, 1-17.

Yizhaq, H., Balmforth, N.J. and Provenzale, A., 2004. Blown by wind: Nonlinear dynamics of aeolian sand ripples. Physica D, 195, 207-228.

Yizhaq, H., Katra, I., Isenberg, O. and Tsoar, H., 2012. Evolution of megaripples from a flat bed, Aeolian Research, 6, 1-12.

Yizhaq, H., Kok, J.F., Katra, I. 2014. Basaltic sand ripples at Eagle crater as indirect evidence for the hysteresis effect in Martian saltation. Icarus 230, 143-150.

Zimbelman, J.R. 2000. Non-active dunes in the Acheron Fossae region of Mars between the Viking and Mars Global Surveyor eras, Geophys. Res. Lett. 27, 1069-1072.

Figures captions

Figure 1. Figure 1. Ripples on Earth and Mars. (a) Normal ripples at Nizzana sand dunes at the western Negev near the border between Israel and Egypt. (b) A sharp transition between almost straight normal ripples (right) and wavy megaripples (left) on the downwind slope of a dune at Sossusvlei, Namibia (the scale bar is 0.5 m long). (c). Two sizes of ripples are evident in this Dec. 13, 2015, view of a top of a Martian sand dune, from NASA's Curiosity Mars rover. (d) Large straight normal ripples at Eldorado crater, Mars.

Figure 2. Fluid threshold velocity as a function of grain size for Earth (red) and Mars (blue) conditions. Both curves show a minimum around 100 μm. The calculations based on Shao and Lu, 2000. Note that the Martian fluid threshold velocity is much higher than that on Earth.

Figure 3. The two profiles used in the ANSYS Fluent simulation for Earth (a) and for Mars (b). The profiles produced by numerical simulations of the ripple model (Eq. 1). Note the Martian ripple is larger (both height and wavelength) than the terrestrial ripple.

Figure 4. Shear velocity over the ripples (in blue) for two wind velocities 10 m/s (red) and 15 m/s (green) for Earth (a) and Mars (b). The dashed line shows the calculated fluid shear velocity threshold velocity based on Shao and Lu, 2000 for 100 μm particles. For Earth conditions the shear velocity is above the fluid threshold velocity at the crest and at part of the windward slope, whereas under Mars conditions $u_* < u_{*_t}$ for the entire ripple profile.

Figure 5. Shear stress over the ripples (in blue) for two wind velocities 10 m/s (red) and 15 m/s (green) for Earth (a) and Mars (b). The dashed line shows the calculated shear stress threshold based on Shao and Lu, 2000 for 100 μm particles. For Earth conditions the shear stress is above the fluid threshold velocity at the crest and at part of the stoss slope, whereas for under Mars conditions the shear stress is below the threshold.

Figure 6. Close up of the vortices that formed between successive ripples for Earth (a) and mars (b) for 15 m/s wind speed.

Figure 7. Streamlines of the flow inside the trough between two successive ripples for Earth (a) and mars (b) for 15 m/s wind speed from left to right.